Journal of Materials Chemistry B

ROYAL SOCIETY OF CHEMISTRY

PAPER

View Article Online
View Journal

Published on 11 November 2020. Downloaded by University of New England on 11/23/2020 3:34:11 AM.

Check for updates

Cite this: DOI: 10.1039/d0tb01766c

Human serum albumin templated MnO_2 nanosheets as an efficient biomimetic oxidase for biomolecule sensing†

Jia Ge,[a] Jian-Hua Yu,[a] Hongfen Yang,*[b] Dan Yang*[c] and Ren Cai*[d]

Received 19th July 2020,
Accepted 11th November 2020

DOI: 10.1039/d0tb01766c

rsc.li/materials-b

Herein, we have proposed a colorimetric biosensor for detection of acid phosphatase based on human serum albumin (HSA) templated MnO_2 nanosheets (HSA-MnO_2 NSs). HSA-MnO_2 NSs as an efficient biomimetic oxidase could catalyze the oxidization of 3,3′,5,5′-tetramethylbenzidine (TMB) to the coloured oxidation product (oxTMB). Acid phosphatase (ACP) could hydrolyze l-ascorbic acid-2-phosphate (AAP) to produce ascorbic acid, and ascorbic acid could lead to the decomposition of MnO_2 NSs to Mn^{2+} ions, inhibiting the production of oxTMB. On the basis of this, we have demonstrated a novel colorimetric approach for the detection of acid phosphatase with the linear range from 50 μU mL^{-1} to 1500 μU mL^{-1} and a detection limit of 40 μU mL^{-1}. The MnO_2 NS-based colorimetric method has been successfully used to determine the content of acid phosphatase in real samples with satisfactory results.

Introduction

Acid phosphatase (ACP), as a ubiquitous hydrolase enzyme, is widely distributed in many mammalian fluids and tissues.[1,2] ACP could catalyze the hydrolysis of phosphate esters under an acidic environment. The imbalance level of ACP is related to the pathophysiological processes of some common diseases, including hepatitis, prostate cancer, acute and multiple myeloma and Gaucher's disease.[3–5] What's more, ACP has been determined by several methods including electrochemical, fluorescence, chromatographic, and immunoassay sensing.[6–11] However, there are certain limitations of the above mentioned methods for acid phosphatase detection, such as high costs, and time consuming and complex operations. Thus, it is of great importance to develop simple, sensitive and specific methods for acid phosphatase activity detection.

Nanomaterial-based enzyme mimics are the subject of current research interest as detection media.[12–15] Natural enzymes are often susceptible to environmental conditions and tend to be digested by protease. Enzyme mimetics having low cost, high stability, and facile synthesis are thus highly desirable.[16,17] Many inorganic nanomaterials, including noble metal nanomaterials, metal oxides, carbon nanomaterials, and cobalt oxyhydroxide possess peroxidase or oxidase-like activity.[18–25] Most of them possess mimic peroxidase activity, but the addition of hydrogen peroxide as the oxidizing agent is required. Very few of them possess oxidase-like catalytic activity and molecular oxygen is often included as the oxidizing agent.

MnO_2 nanosheets (MnO_2 NSs) as a novel 2D nanostructure have attracted considerable attention in bioanalysis owing to their superior large molar extinction coefficient and biological compatibility. MnO_2 NSs have been widely employed in various applications such as supercapacitors, catalysts, and sensors, and in drug delivery.[26–31] Recently, MnO_2 NSs have been reported to possess intrinsic oxidase-like activity, which could directly oxidize 3,3′,5,5′-tetramethylbenzidine (TMB) into a blue oxTMB product, without further addition of hydrogen peroxide.[32] However, TMB-MnO_2 NSs have still received less attention as a convenient detection system.

Herein, we have demonstrated a colorimetric strategy for sensitive and rapid sensing of ACP activity with HSA-MnO_2 NS as a biomimetic oxidase. Compared with MnO_2 NS synthesized from other methods, HSA stabilized MnO_2 NS features good dispersion and stability. As shown in Scheme 1, HSA templated MnO_2 nanosheets could directly oxidize TMB into oxTMB with absorbance at 652 nm. ACP could catalyze the hydrolysis of the ascorbic acid 2-phosphate (AAP) substrate to produce ascorbic acid (AA). MnO_2 NS could be effectively reduced to produce

[a] College of Chemistry, Green Catalysis Center, Zhengzhou University, Zhengzhou 450001, P. R. China
[b] Department of Medicinal Chemistry, Center for Natural Products Drug Discovery and Development (CNPD3), College of Pharmacy, University of Florida, 1345 Center Dr, Gainesville, FL, 32610, USA. E-mail: hongfenyang261@ufl.edu
[c] Centre of Translational Atomaterials, Faculty of Science, Engineering and Technology, Swinburne University of Technology, PO Box 218, Hawthorn, Australia. E-mail: danyang@swin.edu.au
[d] State Key Laboratory for Chemo/Bio-Sensing and Chemometrics, College of Materials Science and Engineering, Hunan University, Changsha 410082, China. E-mail: cairen@hnu.edu.cn

† Electronic supplementary information (ESI) available: Additional figures. See DOI: 10.1039/d0tb01766c

Published on 11 November 2020. Downloaded by University of New England on 11/23/2020 3:34:11 AM.

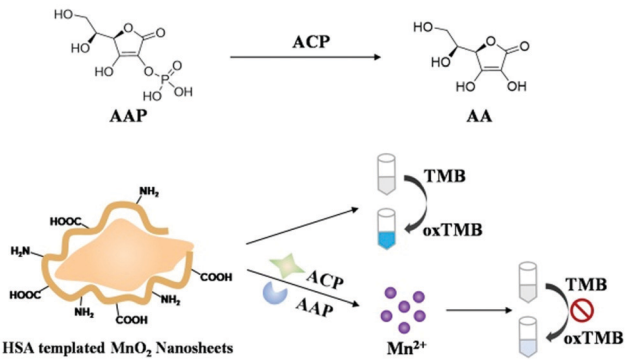

Scheme 1 Schematic representation of the sensing procedure for sensitive ACP detection based on HSA templated MnO_2 nanosheets as a biomimetic oxidase.

Mn^{2+} ions by AA. The absorbance intensity of oxTMB was decreased remarkably as the ACP concentration increased. Therefore, a sensitive and specific colorimetric sensor for the detection of ACP activity can be fabricated based on HSA-MnO_2 NSs. Moreover, this novel platform was also applied for monitoring ACP activity in human serum samples.

Experimental procedures

Synthesis of HSA-MnO_2 NS

In a typical synthesis, 1.0 mL of $MnCl_2$ (0.05 M) was added to 10 mL HSA (1 mg mL^{-1}) solution under continuous stirring, followed by the addition of 0.01 M NaOH solution to adjust the mixture pH value to pH 9.0. Then, the dark brown solution obtained was stirred vigorously for 2 h. The MnO_2 NSs obtained were collected by centrifugation at 12 000 rpm for 30 min and the supernatant was stored at 4 °C for further use.

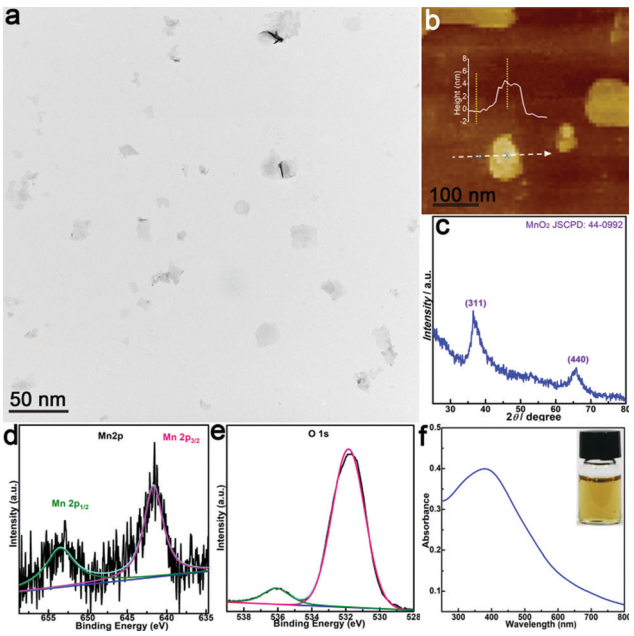

Fig. 1 (a) Typical TEM image of the prepared MnO_2 nanosheets; (b) AFM image; (c) XRD pattern; (d) high-resolution XPS spectra for Mn 2p; (e) high-resolution XPS spectra for O 1s; and (f) UV-vis absorption spectra and photograph of MnO_2 nanosheets.

Detection of ACP activity

To detect ACP activity, 10 μL of different concentrations of ACP, 10 μL of MnO_2 NSs (10 μg mL^{-1}), 10 μL of AAP (100 μM), and 60 μL sodium acetate buffer (0.02 M, pH 4.0) were mixed and kept at 37 °C for 40 min. Then, 10 μL TMB (2 mM) was added. The mixture was incubated at 37 °C for 10 min. Finally, the absorption spectra of different samples were measured at room temperature.

For the selectivity study, several types of biological interferences, including glucose, glucose oxidase (GOx), trypsin, lysozyme, tyrosinase (TRY), and acetyl cholinesterase (AchE), were selected to evaluate the selectivity of the ACP assay. 10 μL of MnO_2 NS (10 μg mL^{-1}), 10 μL of AAP (100 μM), and 10 μL of interfering substances were added into 60 μL sodium acetate buffer (0.02 M, pH 4.0) and kept at 37 °C for 40 min. Then, 10 μL of TMB (2 mM) was added. The mixture was incubated at 37 °C for 10 min. Finally, the absorption spectra of different samples were measured at room temperature.

Results and discussion

Characterization of MnO_2 NS

Herein, HSA was selected as the template for MnO_2 NS synthesis in aqueous solution. As shown in Fig. 1a, the as-synthesized products showed the typical two-dimensional sheets with an average dimension of 100 nm. The structure and thickness of these nanosheets were characterized by atomic force microscopy (AFM). The thickness of one typical nanosheet was measured to be 4.2 nm (Fig. 1b). All the peaks of the X-ray diffraction (XRD) pattern can be identified with the crystal phases of MnO_2 (JCPDS: 44-0992) in Fig. 1c. X-ray photoelectron spectroscopy (XPS) was used to analyze the MnO_2 NSs. The XPS analysis of the resultant MnO_2 NSs showed two peaks centered at 641.2 eV and 653.1 eV that were attributed to Mn $2p_{3/2}$ and Mn $2p_{1/2}$ of MnO_2, respectively (Fig. 1d); the binding energy peaks of O 1s were at 536.1 eV and 531.6 eV, respectively (Fig. 1e). In addition, the as-synthesized MnO_2 NSs were stable in an aqueous solution (inset of Fig. 1f). As shown in Fig. 1f, the absorbance spectrum of the synthesized MnO_2 NSs exhibited a wide band in the range of 250–800 nm with a peak located at 370 nm. These results indicated the successful formation of HSA stabilized MnO_2 NSs.

Monitoring of the ACP

To assess the catalytic properties of the prepared MnO_2 NSs, a classic colorimetric reaction was conducted by a classical oxidase substrate of TMB. As shown in Fig. 2, there was no clear absorption peak at 652 nm with only TMB alone in the solution (curve a in Fig. 2). With the addition of MnO_2 NSs, the color of the solution quickly changed to deep blue and exhibited a strong absorbance at 652 nm (curve e), indicative of

This journal is © The Royal Society of Chemistry 2020

Published on 11 November 2020. Downloaded by University of New England on 11/23/2020 3:34:11 AM.

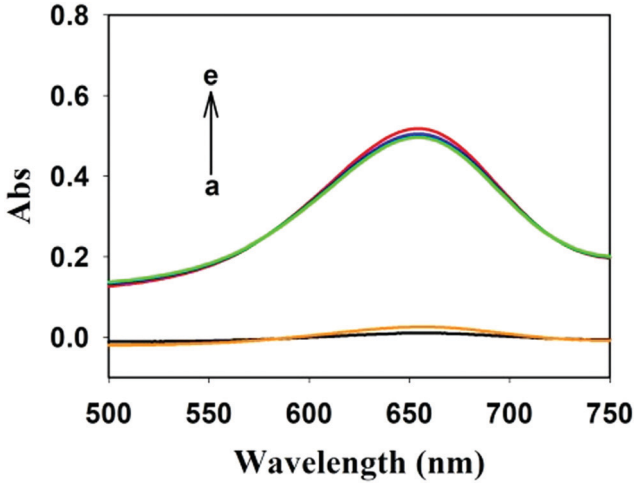

Fig. 2 The absorbance of oxidized TMB at 652 nm. (a) TMB; (b) MnO_2 nanosheets + TMB + ACP + AAP; (c) MnO_2 nanosheets + TMB + AAP; (d) MnO_2 nanosheets + TMB + ACP; (e) MnO_2 nanosheets + TMB.

the formation of the oxTMB and the oxidase-like activity of MnO_2 NSs (Fig. 2). Furthermore, with the addition of AAP and ACP, MnO_2 NSs could be effectively reduced to produce Mn^{2+} ions as ACP could hydrolyze AAP to form ascorbic acid, and the solution became transparent again (curve b in Fig. 2). In contrast, the MnO_2 NSs could catalyze the oxidation of TMB in the solution only containing AAP (curve c in Fig. 2) or ACP (curve d in Fig. 2). These results suggest that the prepared MnO_2 NSs have a peroxidase-like catalysis capability.

Optimization of sensing conditions

In order to obtain the optimal conditions for the colorimetric sensing, we investigated the dependence of many surrounding conditions, such as the solution pH, temperature, the reaction time, and the concentration of TMB. Similarly to natural enzyme-horseradish peroxidase (HRP), the catalytic activity of the prepared MnO_2 NS was directly related to pH value and temperature. As shown in Fig. S1 (ESI†), the oxidase-like activity of HSA-MnO_2 NS was measured with the pH ranging from pH 2 to pH 8. The catalytic activity of HSA-MnO_2 NS was found to increase with pH increased from pH 2 to pH 4, and then decrease with further pH increase from pH 4 to pH 8, which was similar to the behavior of natural peroxidase HRP. Thus, the optimal pH 4.0 was chosen for subsequent experiments. As shown in Fig. S2 (ESI†), the MnO_2 NSs yielded a maximum absorbance at 37 °C when varying the temperature from 4 °C to 70 °C. Therefore, the reaction temperature was selected as 37 °C for subsequent experiments. As shown in Fig. S3 (ESI†), it was observed that the absorbance increased significantly and then reached equilibrium within 10 min. Thus, the optimal reaction time was selected as 10 min. TMB concentration was also considered. As shown in Fig. S4 (ESI†), the results showed that the largest MnO_2 NSs catalytic activity could be obtained by adding 200 μM TMB. Thus, 200 μM TMB was taken as the optimal concentration.

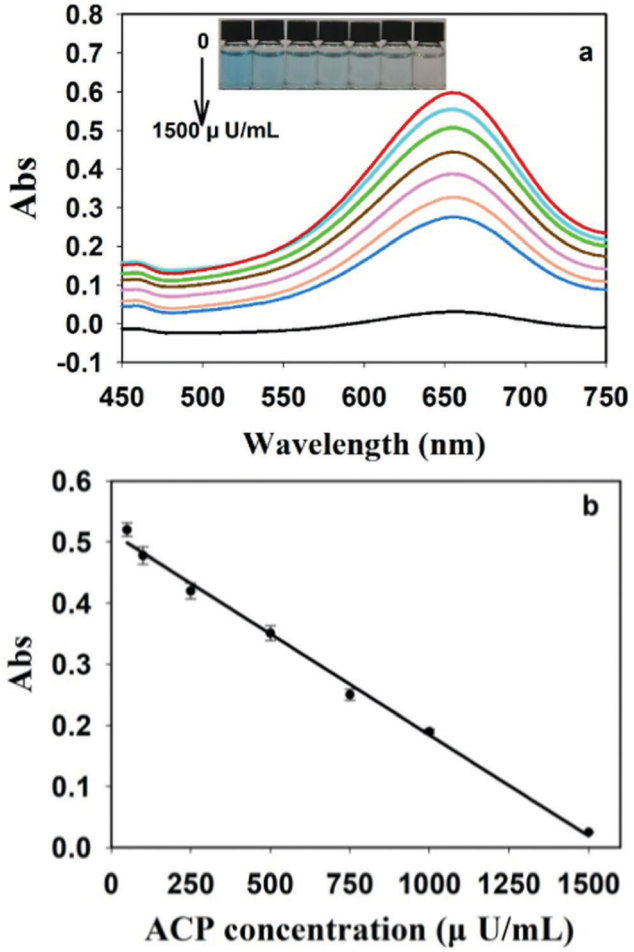

Fig. 3 (a) UV-vis absorption spectra of the assay system in the presence of increasing concentration of ACP, the arrow indicates the signal changes as the concentration of ACP increased (0, 50, 100, 250, 500, 1000, and 1500 μU mL^{-1}). (b) Calibration curve of the assay system for ACP activity detection.

Stability and kinetic analysis of MnO_2 NSs

As shown in Fig. S5 (ESI†), the MnO_2 NSs were dispersed in PBS and human serum for over 48 h without significant aggregation, indicating their good stability. As show in Fig. S6 (ESI†), the steady-state kinetics of MnO_2 NSs catalyzed oxidation of TMB were determined and typical Michaelis–Menten curve were obtained. The K_m and V_{max} values obtained from Lineweaver–Burk plots are displayed in Table S1 (ESI†). MnO_2 NSs showed a smaller K_m value than that of HRP, indicating better affinity between TMB and MnO_2 NS than HRP.[33] In addition, the K_m value of the as-prepared MnO_2 NSs with TMB was lower than other nanomaterial-based oxidase mimics, implying the high affinity of the obtained MnO_2 NSs towards TMB.[34–38]

Detection of ACP using MnO_2 NSs

In order to investigate the practical application of HSA-MnO_2 NSs, we devised a facial colorimetric platform for the detection of ACP activity. As shown in Fig. 3a, the absorbance intensity of oxTMB at 652 nm decreased with the increasing concentration

Published on 11 November 2020. Downloaded by University of New England on 11/23/2020 3:34:11 AM.

Table 1 The comparison of different methods for the detection of ACP

Method	Linear range	LOD	Ref.
Fluorometry	18.2–1300 mU mL^{-1}	5.5 mU mL^{-1}	39
Fluorometry	0–1500 μU mL^{-1}	28 μU mL^{-1}	40
Fluorometry	1–50 μU mL^{-1}	0.45 mU mL^{-1}	41
Magnetoelastic	1.5–15 mU mL^{-1}	1.5 mU mL^{-1}	42
Electrochemical	0.11–5.7 mU mL^{-1}	0.11 mU mL^{-1}	43
Colorimetric	50–1500 μU mL^{-1}	40 μU mL^{-1}	Our work

of ACP from 0 μU mL^{-1} to 1500 μU mL^{-1}. As shown in Fig. 3b, the absorbance intensity showed a good linear relationship with the ACP concentration in the range from 50 μU mL^{-1} to 1500 μU mL^{-1}. The linear regression equation was A652 nm = $-0.0003\ C_{ACP}$ (μU mL^{-1}) + 0.5154, with a correlation coefficient of 0.9973. The limit of detection, defined as a signal-to-noise ratio of S/N = 3, was determined to be 40 μU mL^{-1}. The results show that detection limit of our method is comparable with previous studies,[39–43] as summarized in Table 1.

Evaluation of detection selectivity

The selectivity of this protocol was evaluated by using potential interferences including glucose, GOx, trypsin, lysozyme, TRY, and AchE. As shown in Fig. 4, no significant change was observed with the addition of the potential interferences. Meanwhile, only in the presence of ACP, the absorbance intensity obviously decreased. These results clearly demonstrate the high selectivity for ACP of the proposed protocol.

Determination of ACP activity human serums

The feasibility of the proposed strategy is also tested by the detection of ACP in complex biological samples. In order to test the potential of HSA-MnO_2 NSs for the determination of ACP activity in real samples, the ACP activity in 1% diluted human serum samples were tested using the standard addition method. As shown in Table 2, it was observed that the recovery rate ranged from 96.3% to 98.7%. To test the performance of the proposed strategy in real samples, we applied the sensor to detect ACP activity in PC-3 cell lysates. PC-3 cells, a kind of human prostate cancer cell line, as the model system, were used to investigate the cellular levels of ACP in cells. Moreover, we also used a commercial kit (Acid Phosphatase Colorimetric Assay Kit, Cayman Chemical Company, Michigan, USA) to detect ACP activity in the cell extracts. As shown in Table 3, the results from our assay are in good agreement with those from the commercial kit, indicative of the accuracy and efficiency of our method. The high recovery rate showed the great potential of the proposed method for the detection of ACP in clinical samples.

Table 2 Recovery tests for ACP activity analysis in diluted human serum using the proposed assay (n = 3)

Sample	Added ACP (μU mL^{-1})	Measured (μU mL^{-1})	Recovery (%)
1	50	48.75	97.5
2	100	96.30	96.3
3	200	197.40	98.7

Table 3 Determination of ACP activity in PC-3 cell extracts by comparing the proposed assay and commercial kit

Sample	The proposed method (U mg^{-1} protein)[a]	Commercial kit (U mg^{-1} protein)[a]
Sample 1	1.22 ± 0.03	1.45 ± 0.04
Sample 2	1.16 ± 0.04	1.34 ± 0.02
Sample 3	1.54 ± 0.02	1.62 ± 0.02

[a] Mean of three separate determinations ± standard deviation.

ACP inhibition assay

The assay was also evaluated for testing ACP activity inhibitors since ACP activity inhibitors were potential drugs for treating ACP related diseases. NaF, a well-known ACP inhibitor, was used as a model for inhibition. After the addition of NaF, the ACP activity could be inhibited and the absorbance intensity would increase as expected. The absorbance intensity increased with the increase of NaF concentration, indicating that the

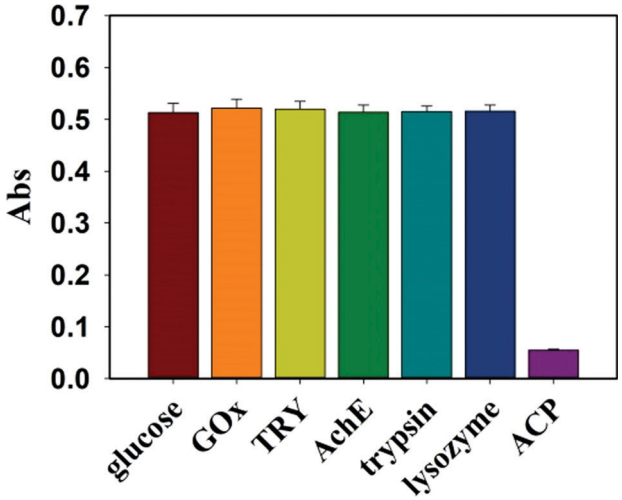

Fig. 4 Selectivity of ACP over potential interferences.

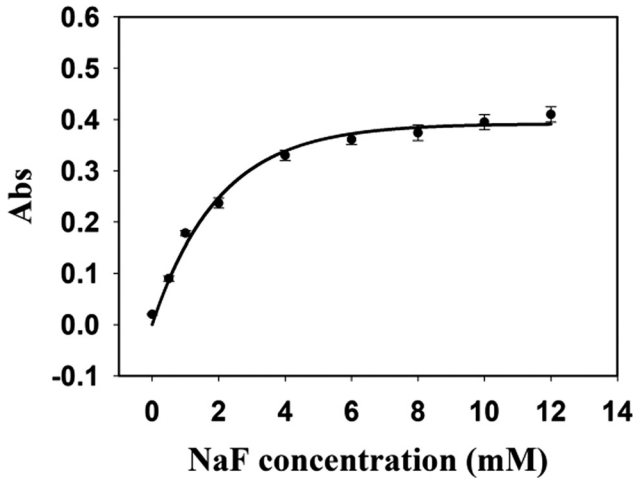

Fig. 5 ACP inhibition efficiency of NaF.

This journal is © The Royal Society of Chemistry 2020

Published on 11 November 2020. Downloaded by University of New England on 11/23/2020 3:34:11 AM.

hydrolysis of AAP by ACP was reduced (Fig. 5). The result indicated that the proposed method could be used for the screening of ACP inhibitors.

Conclusions

In summary, we have developed a new colorimetric strategy for facile sensing of ACP activity with HSA-MnO_2 NSs as an efficient biomimetic oxidase. The HSA-MnO_2 NSs displayed good intrinsic oxidase-like activity with TMB as a peroxidase substrate. Acid phosphatase could catalyze the hydrolysis of the AAP substrate to produce AA. The AA further triggers the decomposition of MnO_2 NSs, which inhibit the generation of oxTMB. Benefiting from the high catalytic activity of MnO_2 NSs, fast-response colorimetric assay has been fabricated for the practical detection of ACP activity with low detection limit and high selectivity. We have also applied this platform for the detection of ACP activity in human blood serum and achieved high recovery rate. The nanosensor proposed in this work shows great potential for the early diagnosis of ACP-related diseases, and could also be applied in other related biological and biomedical fields.

Conflicts of interest

There are no conflicts to declare.

Acknowledgements

This work was supported by the National Natural Science Foundation of China (21505122, 22004032).

Notes and references

1 H. Bull, P. G. Murray, D. Thomas, A. Fraser and P. N. Nelson, *Mol. Pathol.*, 2002, **55**, 65–72.
2 A. V. Taira, G. S. Merrick, K. E. Wallner and M. Dattoli, *Oncology*, 2007, **21**, 1003–1010.
3 S. Veeramani, T. Yuan, S. Chen, F. Lin, J. E. Petersen, S. Shaheduzzaman, S. Srivastava, R. G. MacDonald and M. Lin, *Endocr. Related Cancer*, 2005, **12**, 805–822.
4 B. Kirstein, T. J. Chambers and K. Fuller, *J. Cell. Biochem.*, 2006, **98**, 1085–1094.
5 P. Montesinos, I. Lorenzo, G. Martín, J. Sanz, M. L. Pérez-Sirvent, D. Martínez, G. Ortí, L. Algarra, J. Martínez and F. Moscardó, *Haematol.*, 2008, **93**, 67–74.
6 Z. Fredj, M. B. Ali, M. N. Abbas and E. Dempsey, *Anal. Chim. Acta*, 2019, **1057**, 98–105.
7 F. Shi, Y. Zhang, W. Na, X. Zhang, Y. Li and X. Su, *J. Mater. Chem. B*, 2016, **4**, 3278–3285.
8 Z. Qian, L. Chai, Q. Zhou, Y. Huang, C. Tang, J. Chen and H. Feng, *Anal. Chem.*, 2015, **87**, 7332–7339.
9 Z. Qu, W. Na, X. Liu, H. Liu and X. Su, *Anal. Chim. Acta*, 2018, **997**, 52–59.
10 Y. Yamauchi, M. Ido and H. Maeda, *J. Chromatogr. A*, 2005, **1066**, 127–132.
11 A. H. Kamel, H. R. Galal and A. Hanna, *Int. J. Electrochem. Sci.*, 2014, **9**, 5776–5787.
12 L. Gao, J. Zhuang, L. Nie, J. B. Zhang, Y. Zhang, N. Gu, T. H. Wang, J. Feng, D. L. Yang, S. Perrett and X. Y. Yan, *Nat. Nanotechnol.*, 2007, **2**, 577–583.
13 H. Wei and E. K. Wang, *Chem. Soc. Rev.*, 2013, **42**, 6060–6093.
14 Y. Y. Huang, J. S. Ren and X. G. Qu, *Chem. Rev.*, 2019, **119**, 4357–4412.
15 M. M. Liang and X. Y. Yan, *Acc. Chem. Res.*, 2019, **52**(8), 2190–2200.
16 Y. H. Lin, J. S. Ren and X. G. Qu, *Acc. Chem. Res.*, 2014, **47**, 1097–1105.
17 B. W. Liu and J. W. Liu, *Nano Res.*, 2017, **10**, 1125–1148.
18 Z. Q. Gao, M. D. Xu, L. Hou, G. N. Chen and D. P. Tang, *Anal. Chim. Acta*, 2013, **776**, 79–86.
19 W. W. He, Y. Liu, J. S. Yuan, J. J. Yin, X. C. Wu, X. N. Hu, K. Zhang, J. B. Liu, C. Y. Chen, Y. L. Ji and Y. T. Guo, *Biomaterials*, 2011, **32**, 1139–1147.
20 N. Singh, M. A. Savanur, S. Srivastava, P. D'Silva and G. Mugesh, *Angew. Chem., Int. Ed.*, 2017, **56**, 14267–14271.
21 H. Bagheri, E. Ranjbari, M. Amiri-Aref, A. Hajian, Y. H. Ardakani and S. Amidi, *Biosens. Bioelectron.*, 2016, **85**, 814–821.
22 W. Y. Yin, J. Yu, F. T. Lv, L. Yan, L. R. Zheng, Z. J. Gu and Y. L. Zhao, *ACS Nano*, 2016, **10**, 11000–11011.
23 J. Chen, J. Ge, L. Zhang, Z. H. Li and L. B. Qu, *Sens. Actuators, B*, 2016, **233**, 438–444.
24 H. J. Sun, A. D. Zhao, N. Gao, K. Li, J. S. Ren and X. G. Qu, *Angew. Chem., Int. Ed.*, 2015, **54**, 7176–7180.
25 D. Y. Ji, Y. H. Du, H. M. Meng, L. Zhang, Z. M. Huang, Y. L. Hu, J. J. Li, F. Yu and Z. H. Li, *Sens. Actuators, B*, 2018, **256**, 512–519.
26 W. F. Wei, X. W. Cui, W. X. Chen and D. G. Ivey, *Chem. Soc. Rev.*, 2011, **40**, 1697–1721.
27 M. Safdar, O. M. Wani and J. Jänis, *ACS Appl. Mater. Interfaces*, 2015, **7**, 25580–25585.
28 W. Y. Gao, Z. Y. Liu, L. M. Qi, J. P. Lai, S. A. Kitte and G. B. Xu, *Anal. Chem.*, 2016, **88**, 7654–7659.
29 Q. Y. Cai, J. Li, J. Ge, L. Zhang, Y. L. Hu, Z. H. Li and L. B. Qu, *Biosens. Bioelectron.*, 2015, **72**, 31–36.
30 J. Ge, R. Cai, X. G. Chen, Q. Wu, L. L. Zhang, Y. Jiang, C. Cui, S. Wan and W. H. Tan, *Talanta*, 2019, **195**, 40–45.
31 M. L. Song, T. Liu, C. R. Shi, X. Z. Zhang and X. Y. Chen, *ACS Nano*, 2016, **10**, 633–647.
32 Y. Wan, P. Qi, D. Zhang, J. J. Wu and Y. Wang, *Biosens. Bioelectron.*, 2012, **33**, 69–74.
33 L. Gao, J. Zhuang, L. Nie, J. Zhang, Y. Zhang, N. Gu, T. Wang, J. Feng, D. Yang, S. Perrett and X. Yan, *Nat. Nanotechnol.*, 2007, **2**, 577–583.
34 L. Hu, Y. Yuan, L. Zhang, J. Zhao, S. Majeed and G. Xu, *Anal. Chim. Acta*, 2013, **762**, 83–86.
35 L. Lin, X. Song, Y. Chen, M. Rong, T. Zhao, Y. Wang, Y. Jiang and X. Chen, *Anal. Chim. Acta*, 2015, **869**, 89–95.
36 W. He, X. Han, H. Jia, J. Cai, Y. Zhou and Z. Zheng, *Sci. Rep.*, 2017, **7**, 40103.
37 J. Mu, Y. Wang, M. Zhao and L. Zhang, *Chem. Commun.*, 2012, **48**, 2540–2542.

38 R. J. Cui, Z. D. Han and J. J. Zhu, *Chem. – Eur. J.*, 2011, **17**, 9377–9384.
39 Z. Qian, L. Chai, Q. Zhou, Y. Huang, C. Tang, J. Chen and H. Feng, *Anal. Chem.*, 2015, **87**, 7332–7339.
40 W. D. Na, Q. Liu, B. W. Sui, T. Y. Hu and X. G. Su, *Talanta*, 2016, **161**, 469–475.
41 J. Wang, Y. Yan, X. Yan, T. Hu, X. Tang and X. Su, *Sens. Actuators, B*, 2016, **234**, 470–477.
42 S. Wu, X. Gao, Q. Cai and C. A. Grimes, *Sens. Actuators, B*, 2007, **123**, 856–859.
43 Z. Fredj, M. B. Ali, M. N. Abbas and E. Dempsey, *Anal. Chim. Acta*, 2019, **1057**, 98–105.

Published on 11 November 2020. Downloaded by University of New England on 11/23/2020 3:34:11 AM.

This journal is © The Royal Society of Chemistry 2020